International Journal on Advanced Science Engineering Information Technology

Vol.12 (2022) No. 4
ISSN: 2088-5334

Shortwave Infrared Hyperspectral Imaging for the Determination and Visualization of Chemical Contents of Wheat and Tuber Flour

Rudiati Evi Masithoh [a,*], Lalit M Kandpal [b], Santosh Lohumi [b], Won-Seob Yoon [b], Hanim Zuhrotul Amanah [a,b], Byoung-Kwan Cho [b]

[a] *Department of Agricultural and Biosystems Engineering, Faculty of Agricultural Technology, Universitas Gadjah Mada, Yogyakarta, Indonesia*
[b] *Department of Biosystems Machinery Engineering, College of Agricultural and Life Science, Chungnam, National University, 99 Daehak-ro, Yuseoung-gu, Daejeon 305-764, Republic of Korea*
*Corresponding author: *evi@ugm.ac.id*

Abstract— **Understanding the physicochemical properties of flour in food preparation is important to determine the appropriate food utilization and processing. Some crops are processed into flour to improve their shelf life and extend their applications in food preparation. This study employed shortwave infrared hyperspectral imaging (SWIR HSI) coupled with multivariate analyses to determine wheat's protein, starch, amylose, glucose, and moisture compositions and several tuber flours. Tubers used were arrowroot, Canna edulis, modified cassava flour, taro, and sweet potato (purple, yellow, and white color). Hyperspectral images of all flour samples were captured using the SWIR HSI system at the wavelength range of 895–2504 nm in reflectance mode. The extracted spectral data were then processed and analyzed using partial least square regression (PLSR). Normalization (mean, max, and range), multiple scatter correction, standard normal variate, first and second Savitzky–Golay derivatives, and smoothing spectral pre-processing were applied to reduce scattering noise resulting from the HSI system. The PLSR models predicted the chemical concentrations of all samples with coefficients of determination of 0.85-0.97, 0.83-0.96, and 0.85-0.96 for calibration, validation, and prediction, respectively. Moreover, the models resulted in standard errors of 0.61-27.26, 0.63-27.71, and 0.63-29.14 for calibration, validation, and prediction. The concentration and distribution of protein, starch, amylose, glucose, and moisture in the flour samples were visualized by chemical imaging. This paper confirmed the potential of HSI for the rapid interpretation of chemical contents in different flour samples.**

Keywords— **Shortwave infrared; hyperspectral imaging; wheat; tuber; protein; starch; amylose; glucose; moisture.**

Manuscript received 18 Jan. 2021; revised 13 Apr. 2021; accepted 15 May 2021. Date of publication 31 Aug. 2022.

I. INTRODUCTION

Wheat is a popular crop in food production, especially in bread and noodle making. Although wheat is not of Indonesian origin, Indonesians consume wheat-based products as an alternative to rice. In 2019–2020, Indonesia is estimated to import around 11.2 million tons of wheat [1]. Despite the high demand for wheat, Indonesia and other tropical countries have abundant tuber crops, such as cassava, canna, sweet potato, arrowroot, and taro which are a source of carbohydrates.

Wheat and tubers are commonly processed into flour to prolong their self-life and improve their application. With high nutritional values of wheat and tubers, their flour forms are beneficially utilized in the food industry. Although many types of flour are available, their suitability for certain applications requires understanding their physicochemical properties. For example, given their low protein content, tuber crops are usually prepared as gluten-free products suitable for people allergic to gluten [2]. In addition, understanding the physicochemical properties of flour is important to determine the appropriate food processing.

The major physicochemical properties of flour, including protein, starch, amylose, glucose, and moisture, are commonly determined using destructive methods. Those methods involve extensive amounts of laboratory work so impractical for routine and large samples. Thus, a rapid and non-destructive method must be developed to obtain flour's physicochemical properties, which is very useful in food manufacturing and processing.

Hyperspectral imaging (HSI) simultaneously utilizes spectroscopy and imaging data to acquire spatial and spectral information. Therefore, it has the potential to describe the

distribution of sample constituents. HSI has been applied to authenticate or detect the presence of additives or foreign materials in milk [3], wheat flour [4], green coffee [5], or oats [6]. HSI has also been applied to predict the chemical composition of maize seeds [7], the solid soluble content of apples [8], and the moisture content of tea leaves [9]. However, few studies have been conducted to determine the chemical compositions (such as protein, starch, amylose, glucose, and moisture) of wheat and tuber flour by using the HSI. The chemical composition information obtained from the HSI is important in providing rapid quantitative and qualitative judgment for the food industry.

Therefore, the potential of HSI to determine the protein, starch, amylose, glucose, and moisture contents of wheat and several tuber flours was evaluated in this study. This study develops partial least square regression (PLSR) models to predict the chemical contents of wheat and tuber flour. It also creates images to visualize protein, starch, amylose, glucose, and moisture in wheat and tuber flour based on the best PLSR model.

II. Material and Method

A. Sample Preparation and Chemical References Determination

Samples used in this study consisted of eight various flour, namely, wheat, arrowroot (*Maranta arundinacea*), cassava (*Manihot esculenta*), taro (*Colocasia esculenta*), *Canna edulis* (*Canna indica*), and purple, yellow, and white sweet potato (*Ipomoea batatas*). All samples were obtained from several sellers in Indonesia. Flour samples were dried in a 50°C dryer for 24 h and filtered with a 212 µm sieve to obtain moisture and particle size uniformity.

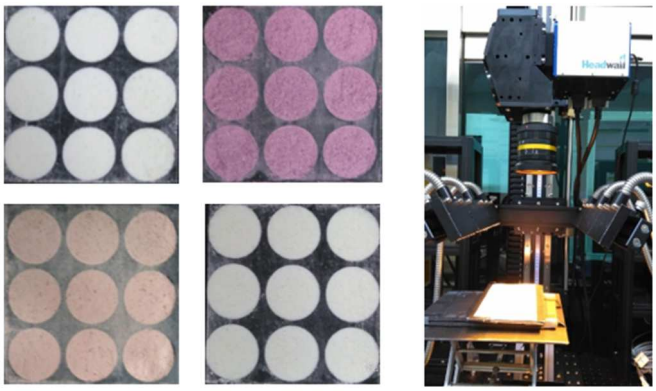

(a) (b)

Fig. 1 (a) Samples used: From left: Taro and purple sweet potato flour (top), yellow sweet potato and arrowroot flour (bottom), (b) line scan SWIR hyperspectral imaging system

Each flour was placed in a sample holder plate as shown in Figure 1(a) containing nine samples of each flour for HSI scanning. Protein was determined with the standard Kjeldahl method using FOSS TECATOR Kjeltec Auto 1030 Analyzer (FOSS, Denmark). Glucose content (in µg/g) was determined using the HPLC method using CarboPac ™ (PAI (4 x 250 mm), P/N 35391, USA). Starch (in %) and amylose (in %) were determined previously described [10], whereas moisture (in %) was measured using the common gravimetric method. The standard of deviation (SD), maximum (max), and minimum (min) of chemical compositions of wheat and tuber flour used in this study are shown in Table 1.

TABLE I
CHEMICAL COMPOSITIONS OF WHEAT AND TUBER FLOUR

Component		Protein %	Starch %	Amylose %	Glucose (µg/g)	Moisture %
CA	Mean	0.10	43.14	43.26	24.38	16.68
	SD	0.07	2.25	2.13	20.84	0.62
	Max	0.24	47.22	46.61	59.50	17.40
	Min	0.04	40.43	40.41	7.36	15.60
AR	Mean	0.07	38.87	43.59	36.32	17.23
	SD	0.06	9.37	2.63	38.26	1.52
	Max	0.18	45.73	45.63	147.72	18.64
	Min	0.01	19.10	38.05	11.52	13.64
MC	Mean	1.04	18.05	33.68	258.58	13.50
	SD	0.33	3.80	1.84	90.64	1.05
	Max	1.57	22.11	36.92	365.16	15.04
	Min	0.68	11.66	31.13	112.40	11.78
TR	Mean	7.24	22.00	24.29	4.76	12.76
	SD	2.81	4.39	4.16	1.05	0.19
	Max	10.08	28.23	29.31	6.09	13.00
	Min	4.40	14.58	19.58	3.06	12.26
WSP	Mean	3.11	12.40	28.19	32.89	10.10
	SD	0.43	2.40	2.55	7.52	0.60
	Max	3.93	16.31	31.76	42.36	11.14
	Min	2.60	8.08	25.00	22.38	9.10
YSP	Mean	3.27	5.66	20.99	58.52	9.58
	SD	0.49	0.97	1.64	9.00	0.79
	Max	3.82	7.38	23.10	69.26	10.88
	Min	2.77	4.01	17.44	46.36	8.24
PSP	Mean	3.71	8.91	26.02	23.43	10.00
	SD	0.69	2.45	3.09	12.32	0.63
	Max	4.84	12.64	32.38	53.01	11.16
	Min	2.83	4.14	22.05	11.47	9.24
WH	Mean	11.17	20.49	37.65	0.85	13.63
	SD	1.60	3.48	1.13	0.18	0.27
	Max	13.62	27.67	40.44	1.09	13.97
	Min	7.86	15.71	36.46	0.51	13.25

Note: CA = *Canna edulis*; AR = arrowroot; MC = modified cassava; TR = taro; WH = wheat; PSP = purple sweet potato; WSP = white sweet potato; YSP = yellow sweet potato

B. Shortwave Infrared (SWIR) Hyperspectral Imaging (HSI) System

The line-scan SWIR HSI system used in this study is similar to the one reported by Rahman et al [11], shown in Figure 1(b). The system consisted of a spectrograph (Headwall Photonics, Fitchburg, MA, USA), six of 100 W tungsten-halogen lamps (Light Bank, Ushio Inc., Japan), a mercury cadmium telluride detector, a SWIR camera sized 320 x 256 pixels (Headwall Photonics, Fitchburg, MA, USA), and 1.4/25 C-mount lens (Navitar, SWIR-25, Rochester, NY, USA). The HSI system was also equipped with a stepper motor, spectra and image acquisition software, and a display monitor. The spectral range at 895–2504 nm and an interval of 5.85 nm resulted in 275 variables for multivariate analysis.

C. Hyperspectral Image Acquisition

Ten plates of each flour were placed in the sample plate and scanned for image acquisition in reflectance mode, producing 720 spectra. One at a time, the plate was placed on the conveyor table (Xslide, Velmex Inc., Bloomfield, NY, USA), which moved the plate in the view range of the hyperspectral

camera. The movement was controlled by the step interval and the step number. Line-by-line sample scanning was performed during conveyor movement to obtain spectral and spatial data. The conveyor movement and the exposure time were set at 5.869 mm/s and 40.42 ms, respectively, to improve the signal-to-noise ratio. The distances of camera to samples and the lamps to samples were 21 and 12.5 cm, respectively.

The samples were scanned line-by-line using the hyperspectral camera in the short-wave infrared range of 895–2504 nm, and images were collected in reflectance mode. The hyperspectral images were then saved as 3-dimension hypercubes which comprised 2-spatial (320 x n pixels in the x and y-direction) and 1-spectral (275 bands in the k-direction) dimensions. The obtained 3D images were corrected using white and dark references. The white reference images were obtained by a white Teflon sheet which had >99% reflectance, while dark reference images (>0% reflectance) were obtained by covering the camera with a cap with the light off. Those white and dark images were used to reduce noise resulted from illumination, detector, and geometry [12]. The system and image acquisition were controlled by the self-developed software based on Microsoft Visual Basic (Version 6.0) in the MS Windows system.

D. Spectral Processing

Figure 2 shows the key procedures for the acquisition and visualization of chemical compositions in wheat and tuber flour. These procedures included hyperspectral image acquisition, image extraction, PLSR model development, and chemical-map visualization. Of all images captured from the HSI system, only selected spectra obtained from the region of interest (ROI) were used for spectral pre-processing, multivariate analysis, and chemical-map visualization. The mean, max, and range normalization, multiple scatter correction (MSC), standard normal variate (SNV), first and second Savitzky–Golay derivatives, and smoothing, were applied to the hypercube raw data to reduce scattering noise from the HSI system. ROI selection and spectral pre-processing were developed using MATLAB (The Math Works, Natick, MA, USA).

E. Multivariate Analysis and Chemical Visualization Map

Principal component analysis (PCA) was used to visualize large variable data, whereas PLSR was used to analyze spectroscopic data consisting of large, noisy, and multicollinear independent variables. In PCA, the original spectra were converted into several principal components to represent spectral variations, which produced a robust model for the prediction of complex samples. A PLSR model was developed to determine wheat and tuber flour's protein, starch, amylose, glucose, and moisture contents. In this study, the X-variable was absorbance values, whereas the Y-variable was the chemical content. The PLSR model resulted in latent variables used to predict Y-variables. Full cross-validation (leave-one-out) method was employed to avoid overfitting of the PLSR model.

Several PLSR models were developed using X-variables that were processed using several pre-processing methods. The performance of PLSR models was assessed based on the coefficient of determination of calibration, cross-validation, and prediction, which were denoted as R_c^2, R_{cv}^2, and R_p^2, respectively. The performance was also assessed based on the standard errors of calibration, cross-validation, and prediction denoted as SEC, SECV, and SEP, respectively.

The PLSR results were converted into images to identify the protein, starch, amylose, glucose, and moisture contents. The beta coefficients from the selected PLSR model were applied to visualize each pixel in hyperspectral images. Spectral processing, multivariate analysis, and visualization map were performed using MATLAB software (The Math Works, Natick, MA, USA).

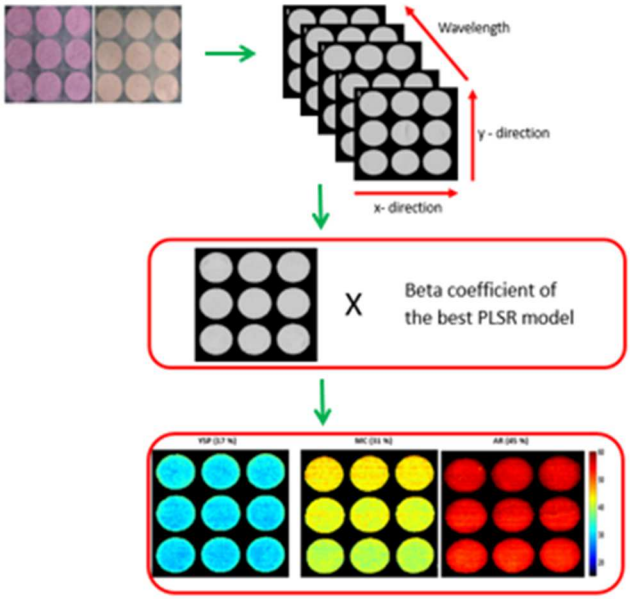

Fig. 2 Measurement and visualization of chemical compositions in wheat and tuber flour

III. Results and Discussion

A. Spectral Characteristics

Original spectra of all samples in the wavelength of 1000–1800 nm was similar for all samples (figure was not included); thus, the samples were not easily differentiated. Spectra of each sample were averaged to obtain the mean spectra, which are clearly illustrated in Figure 3(a). Modified cassava and *Canna edulis* flour had the highest and lowest intensity values, respectively, whereas the other flour was in between. The figure shows a significant peak at around 1400–1500 nm, which corresponded to O-H stretch and O-H first overtone, C-H combination, C=O stretch third overtone, and N-H first overtone.

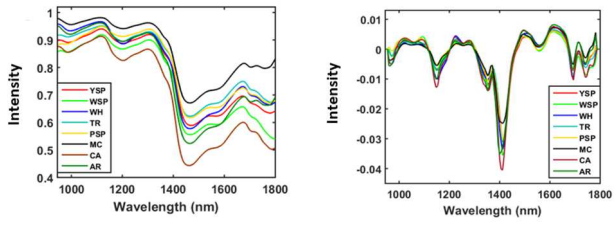

Fig. 3 (a) Mean of original spectra (b) Mean of 1st Savitkzy–Golay derivative pre-processed spectra of all flour samples

After applying the first Savitzky–Golay derivative, mean spectra are illustrated in Figure 3(b), in which more distinct

peaks appeared compared with the original spectra. The figures show significant peaks at around 1100-1200 nm, which corresponded to C-H second overtone, C=O stretch fourth overtone, and C-H second overtone, at 1300-1400 nm, which corresponded to C-H combination, and at 1700-1800 nm, which corresponded to C-H stretch first overtone and O-H combination.

B. Multivariate Analysis

The multilinear regression models in this study were developed using all 720 spectra of all flour samples. As an alternative to developing one model for each flour, this study developed models by incorporating all flour samples. Descriptive data of chemical content of all samples are shown in Table 2, showing a number of samples, as well as statistical values of chemical contents used as calibration and validation sets.

TABLE II
DESCRIPTIVE STATISTICS FOR CALIBRATION AND VALIDATION SETS FOR DIFFERENT COMPONENTS

Component		No. of sample	Min	Max	Range	Mean ± SD
Protein	Cal	497	0.01	13.62	13.61	3.67 ± 3.74
(710)*	Val	213	0.01	13.62	13.61	3.71 ± 3.84
Starch	Cal	497	4.01	47.22	43.21	21.26 ± 13.54
(709)*	Val	212	4.01	47.22	43.21	21.26 ± 13.05
Amylose	Cal	486	17.44	46.61	29.16	32.00 ± 8.62
(695)*	Val	209	17.44	46.09	28.65	32.56 ± 8.15
Glucose	Cal	486	0.50	365.15	364.65	46.30 ± 70.71
(692)*	Val	206	0.50	352.02	351.51	49.65 ± 77.38
Moisture	Cal	504	8.24	18.64	10.40	12.92 ± 2.86
(720)*	Val	216	8.24	18.64	10.40	12.94 ± 2.92

Note: Min=minimum; Max=maximum; Cal=calibration; Val=validation; SD=deviation standard
*Total number of samples after outlier removal is indicated in parentheses

This study used PCA and Hotelling T2 and Q residual plots to detect any possible outliers. These unsupervised techniques can detect outliers based on spectral characteristics. The spectra that did not match with the other spectra of samples from the same group were regarded as outliers. Figure 4 shows the PCA score plot and Hotelling T^2 and Q residual plots for all samples.

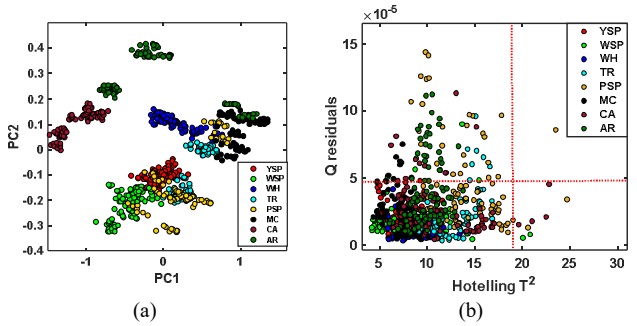

(a) (b)

Fig. 4 (a) PCA score plot, and (b) Hotelling T^2 and Q residual plot for all data set (720 samples)

The PCA score plot is used to observe natural grouping among different varieties of samples and any possible outlier detection. In general, as shown in Figure 4(a), each sample was clearly grouped, but some tubers were mixed up with other tuber samples. For example, TR mixed up with YSP and PSP, or TR mixed up with MC. The phenomenon might be due to tubers' similar chemical characteristics, which mainly consisted of carbohydrates. It can also be observed that wheat (WH) flour, which is not a tuber, is clearly separated from other tuber flour samples. The Hotelling T^2 plot is shown in Figure 4(b) can also be used to detect outliers. Some outliers were detected from the Hotelling T^2 plot, such as some samples of PSP, TR, and AR flour. The variety of the samples possibly caused the outliers.

C. PLSR Analysis

Table 3 shows the best PLSR calibration models for determining chemical contents selected from the highest R_c^2 and the lowest SEC. The best calibration models obtained resulted in R_c^2 of 0.97 for protein, 0.93 for starch, 0.95 for amylose, 0.85 for glucose, and 0.95 for moisture, respectively. The best calibration models also resulted in SEC of 0.64 for protein content, 3.56 for starch content, 1.96 for amylose content, 27.26 for glucose content, and 0.61 for moisture content. All the best PLSR calibration models resulted from first and second Savitkzy–Golay derivative pre-processing spectra. The derivative method was able to resolve problems arising from the instrument or samples by undertaking overlapping signals, improving signal properties, and eliminating undesirable spectral features [13].

TABLE III
PLSR RESULTS FOR DIFFERENT CHEMICAL COMPONENTS IN FLOUR SAMPLES FROM THE METHOD

Component	Calibration		Cross-validation		Prediction		Pre processing
	R_c^2	*SEC*	R_{cv}^2	*SECV*	R_P^2	*SEP*	
Protein	0.97	0.64	0.96	0.68	0.96	0.73	2nd SGD
Starch	0.93	3.56	0.96	3.62	0.96	3.52	1st SGD
Amylose	0.95	1.96	0.94	2.04	0.93	2.21	1st SGD
Glucose	0.85	27.26	0.83	27.71	0.85	29.14	1st SGD
Moisture	0.95	0.61	0.95	0.63	0.95	0.63	2nd SGD

Note: SGD= Savitkzy–Golay derivative

When the best model was applied to predict protein content, it resulted in R_p^2 of 0.96 and SEP of 0.73. Other studies obtained R_c^2 and SEC of 0.99 and 0.34 [14] and R_p^2 and SEP of 0.97–0.99 and 0.07–0.21, respectively [15]. The best calibration models obtained were applied to prediction data sets, resulting in R_p^2 of 0.96, 0.93, 0.85, and 0.95 for predicting starch, amylose, glucose, and moisture contents, respectively. The models also resulted in SEP of 3.52, 2.21, 29.14, and 0.63 for predicting starch, amylose, glucose, and moisture contents. The developed models for amylose and starch determination in this study were consistent with findings that reported coefficients of determination (R^2) of 0.97 and 0.88 for amylose and starch in pea flour [16], and R^2 value of 0.94 for amylose in rice [17]. The model for predicting glucose was adequate but lower than findings obtained for Morinda radix [18] and lotus root powder [19], which had R^2 higher than 0.90. The best calibration model was satisfactory for predicting moisture content with R_p^2 of 0.95 and SEP of 0.63, similar to the quantification of moisture in cocoa powder [20]. The PLSR results implied that the HSI system is sufficient for determining the chemical contents of flour samples.

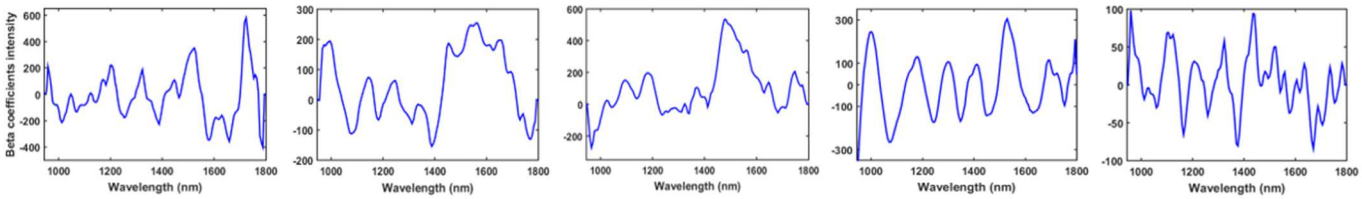

Fig. 5 Beta coefficients of (a) protein, (b) starch, (c) amylose, (d) glucose, and (e) moisture resulted from PLS regression

Figure 5 shows the beta coefficient values of protein, starch, amylose, glucose, and moisture resulting from PLS regression using hyperspectral images. The beta coefficients resulting from PLS regression can be used to analyze the relationship between spectra at different wavelengths and the chemical information of components. Figure 5(a) shows several distinct peaks with high beta regression coefficients at 960 nm related to O-H, and at 1470, 1520, 1570, 1660, 1720, and 1780 nm assigned to N-H stretch first overtone and C-H stretch first overtone, which might be related to proteins, similar to previously reported findings [21], [22]. Table 1 shows variations of protein contents of all flour samples in which wheat is the highest and is the lowest.

In Figure 5(b), some significant peaks could be observed at 1090 nm of O-H bands [23], 1390 nm of C-H combination, 1450 and 1540 nm of O-H stretch overtone, and 1765 nm of C-H stretch first overtone, which might be assigned to starch, similar to previously reported findings [24] at 1040-1200 nm of C-H stretching. Several peaks in developing the amylose calibration model were detected at 1170, 1470, and 1750 nm, which corresponded to C-H second overtone, N-H stretch first overtone, and C-H stretch first overtone, as shown in Figure 5(c). Those significant bands are similar to the ones used in developing the amylose model of rice flour at 1228 and 1540 nm and pea flour at 1426 nm [16], [25]. Similar peaks observed in amylose were also found in starch because amylose was part of polymers in starch [26] and thus featured similar chemical structures. A previous study [10] reported the same peaks affecting the development of starch and amylose models at 1395, 1908, and 2258 nm when measured using near-infrared spectroscopy.

Figure 5(d) illustrates the regression coefficients for determining glucose which showed significant bands at 1000 and 1080 nm of O-H bands, 1180, 1247, 1300, and 1353 nm of C-H second overtone and combination; 1410 and 1450 nm of O-H first overtone and O-H stretch first overtone; 1520 nm of N-H stretch first overtone; 1620 1640, 1688, and 1760 nm of C-H stretch first overtone. Ref [27] marked significant bands at 1706, 1910, 2283, and 2345 nm used in developing the glucose model. Although treated with drying prior to spectral acquisitions, the moisture content in the flour samples was still high with variations of 2.87 % - 18.64 %, which might affect the chemical calibration models. When a model for predicting the moisture was developed, the results are shown in Figure 5(e). The figure shows several significant peaks at 960, 1106, 1450, and 1540 nm, which corresponded to O-H band overtones. However, other molecules also appeared at 1165 nm of C-O stretch, 1324 and 1377 of C-H combinations, and 1670 nm of C-H stretch first overtone. In addition, a previous study [28] reported several wavelengths at 977, 1071, 1198, 1265, 1396, and 1453 nm for potato and 974, 1071, 1202, 1265, 1399, and 1456 nm for sweet potato by using HSI for tuber grading based on moisture content.

Those results suggested that the HSI system generates several significant bands similar to those obtained using the common FT-NIR or FT-IR instruments. The bands are important in developing a calibration model for predicting the chemical contents of flour. Therefore, the beta coefficients obtained from the HSI system in this study are adequate to create the chemical concentration maps.

D. Chemical concentration maps

The HSI method is usually accompanied by chemical concentration maps generated using beta coefficients obtained from the PLSR models [11]. In this study, the chemical concentration maps were made for each chemical component to show the effectiveness of HSI for the visualization of different chemical components in different flour samples.

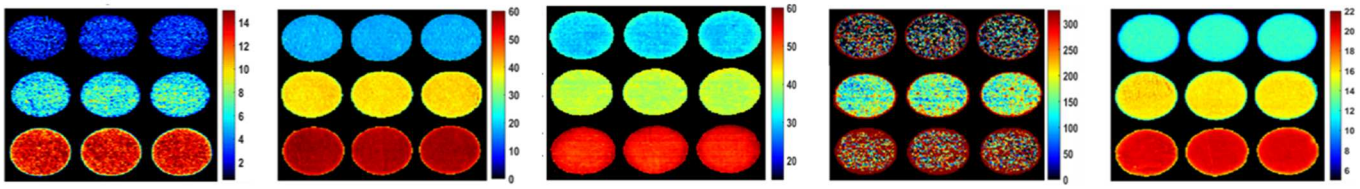

Fig. 6 Concentration map of different components in powder samples generated using the beta coefficients obtained from the developed PLSR models, for (a) protein, (b) starch, (c) amylose, (d) glucose, and (e) moisture

Figures 6(a), 6(b), 6(c), 6(d), and 6(e) show the visualization of protein, starch, amylose, glucose, and moisture concentrations of several flour obtained from the PLSR chemical images. Those images provided the spatial distribution and chemical concentration of the flour. The maps could be used to ease and fasten in determining the chemical composition and are beneficial for grading purposes. Figures 6(a), 6(b), 6(c), and 6(e) are filled with consistent colors which showed more homogeneous concentrations of protein, starch, amylose, and moisture in each flour compared with glucose. The concentration map of glucose in Figure 6(d) shows some mixed-up colors, indicating that the concentration of glucose varied even in one type of flour, which affected the development of the model. As listed in Table 3, the calibration and prediction models for glucose had the lowest performance.

IV. Conclusion

Few studies were conducted to determine the chemical composition of flour samples using shortwave infrared hyperspectral imaging (SWIR-HSI); therefore, it was explored in this research. This study confirmed the potential of the SWIR-HSI for determining protein, starch, amylose, glucose, and moisture contents of wheat and tuber flour with relatively high accuracy. The PLSR produced calibration models with R_c^2 ranging from 0.85 – 0.97 and SEC ranging from 0.61 – 27.26. Moreover, the prediction models produced R_p^2 ranging from 0.85 – 0.96 and SEP ranging from 0.63 – 29.14. Based on the PLSR models, the HSI system best-predicted protein content and the least for predicting glucose content.

Using beta coefficients resulting from the PLSR models, chemical concentration maps were generated. The developed concentration maps provided rapid visualization of flour samples' protein, starch, amylose, glucose, and moisture content. The study underlined the ability of the developed imaging-based technique to predict the chemical content of flour samples. A similar technique can be used for predicting other flour samples or chemical contents. This technique provides automated and real-time data collection and analysis, facilitating rapid analysis in the food industry.

Acknowledgment

This research was funded by the Next-Generation BioGreen 21 Program (No. PJ01311303), Rural Development Administration, South Korea.

References

[1] FAO, "GIEWS - Global Information and Early Warning System," 2019. [Online]. Available: http://www.fao.org/giews/countrybrief/country.jsp?code=IDN.

[2] P. Jnawali, V. Kumar, and B. Tanwar, "Celiac disease: Overview and considerations for development of gluten-free foods," *Food Sci. Hum. Wellness*, vol. 5, no. 4, pp. 169–176, 2016.

[3] D. A. P. Forchetti and R. J. Poppi, "Use of NIR hyperspectral imaging and multivariate curve resolution (MCR) for detection and quantification of adulterants in milk powder," *LWT - Food Sci. Technol.*, vol. 76, pp. 337–343, 2017.

[4] S. Lohumi, H. Lee, M. S. Kim, J. Qin, and B. K. Cho, "Raman hyperspectral imaging and spectral similarity analysis for quantitative detection of multiple adulterants in wheat flour," *Biosyst. Eng.*, vol. 181, pp. 103–113, 2019.

[5] P. Oliveri, C. Malegori, M. Casale, E. Tartacca, and G. Salvatori, "An innovative multivariate strategy for HSI-NIR images to automatically detect defects in green coffee," *Talanta*, vol. 199, no. October 2018, pp. 270–276, 2019.

[6] C. Erkinbaev, K. Henderson, and J. Paliwal, "Discrimination of gluten-free oats from contaminants using near infrared hyperspectral imaging technique," *Food Control*, vol. 80, pp. 197–203, 2017.

[7] G. Yang, Q. Wang, C. Liu, X. Wang, S. Fan, and W. Huang, "Rapid and visual detection of the main chemical compositions in maize seeds based on Raman hyperspectral imaging," *Spectrochim. Acta - Part A Mol. Biomol. Spectrosc.*, vol. 200, pp. 186–194, 2018.

[8] C. Mo *et al.*, "Spatial assessment of soluble solid contents on apple slices using hyperspectral imaging," *Biosyst. Eng.*, vol. 159, pp. 10–21, 2017.

[9] J. Sun, X. Zhou, Y. Hu, X. Wu, X. Zhang, and P. Wang, "Visualizing distribution of moisture content in tea leaves using optimization algorithms and NIR hyperspectral imaging," *Comput. Electron. Agric.*, vol. 160, no. June 2018, pp. 153–159, 2019.

[10] R. E. Masithoh, S. Lohumi, W. Yoon, H. Z. Amanah, and B. Cho, "Development of multi-product calibration models of various root and tuber powders by fourier transform near infra-red (FT-NIR) spectroscopy for the quantification of polysaccharide contents," *Heliyon*, vol. 6, no. 10, p. e05099, Oct. 2020.

[11] A. Rahman, L. M. Kandpal, S. Lohumi, M. S. Kim, and H. Lee, "Nondestructive Estimation of Moisture Content , pH and Soluble Solid Contents in Intact Tomatoes Using Hyperspectral Imaging," *Appl. Sci.*, no. January, 2017.

[12] S. Teerachaichayut and H. T. Ho, "Non-destructive prediction of total soluble solids, titratable acidity and maturity index of limes by near infrared hyperspectral imaging," *Postharvest Biol. Technol.*, vol. 133, no. March, pp. 20–25, 2017.

[13] B. Zimmermann and A. Kohler, "Optimizing Savitzky-Golay parameters for improving spectral resolution and quantification in infrared spectroscopy," *Appl. Spectrosc.*, vol. 67, pp. 892–902, Aug. 2013.

[14] M. Başlar and M. F. Ertugay, "Determination of protein and gluten quality-related parameters of wheat flour using near-infrared reflectance spectroscopy (NIRS)," *Turkish J. Agric. For.*, vol. 35, no. 2, pp. 139–144, 2011.

[15] D. Ye, L. Sun, B. Zou, Q. Zhang, W. Tan, and W. Che, "Non-destructive prediction of protein content in wheat using NIRS," *Spectrochim. Acta Part A Mol. Biomol. Spectrosc.*, vol. 189, pp. 463–274, 2018.

[16] L. Zeng and C. Chen, "Simultaneous estimation of amylose, resistant, and digestible starch in pea flour by visible and near-infrared reflectance spectroscopy," *Int. J. Food Prop.*, vol. 21, no. 1, pp. 1129–1137, 2018.

[17] P. S. Sampaio, A. Soares, A. Castanho, A. S. Almeida, J. Oliveira, and C. Brites, "Optimization of rice amylose determination by NIR-spectroscopy using PLS chemometrics algorithms," *Food Chem.*, vol. 242, pp. 196–204, 2018.

[18] Q. Hao *et al.*, "Prediction the contents of fructose , glucose , sucrose , fructo- oligosaccharides and iridoid glycosides in Morinda of ficinalis radix using near-infrared spectroscopy," *Spectrochim. Acta Part A Mol. Biomol. Spectrosc.*, vol. 234, 2020.

[19] N. Xiaoying, Z. Zhilei, J. Kejun, and L. Xiaoting, "A feasibility study on quantitative analysis of glucose and fructose in lotus root powder by FT-NIR spectroscopy and chemometrics," *Food Chem.*, vol. 133, no. 2, pp. 592–597, 2012.

[20] A. Veselá, A. S. Barros, A. Synytsya, I. Delgadillo, J. Čopíková, and M. A. Coimbra, "Infrared spectroscopy and outer product analysis for quantification of fat, nitrogen, and moisture of cocoa powder," *Anal. Chim. Acta*, vol. 601, no. 1, pp. 77–86, 2007.

[21] L. S. Magwaza, S. I. Messo Naidoo, S. M. Laurie, M. D. Laing, and H. Shimelis, "Development of NIRS models for rapid quantification of protein content in sweetpotato [Ipomoea batatas (L.) LAM.]," *LWT - Food Sci. Technol.*, vol. 72, pp. 63–70, 2016.

[22] M. A. Quelal-Vásconez, M. J. Lerma-García, É. Pérez-Esteve, A. Arnau-Bonachera, J. M. Barat, and P. Talens, "Fast detection of cocoa shell in cocoa powders by near infrared spectroscopy and multivariate analysis," *Food Control*, vol. 99, no. December 2018, pp. 68–72, 2019.

[23] X. Jin *et al.*, "Determination of hemicellulose, cellulose and lignin content using visible and near infrared spectroscopy in Miscanthus sinensis," *Bioresour. Technol.*, vol. 241, pp. 603–609, 2017.

[24] Y. Bantadjan, R. Rittiron, K. Malithong, and S. Narongwongwattana, "Establishment of an accurate starch content analysis system for fresh cassava roots using short-wavelength near infrared spectroscopy," no. June, 2020.

[25] L. H. Xie *et al.*, "Optimisation of near-infrared reflectance model in measuring protein and amylose content of rice flour," *Food Chem.*, vol. 142, pp. 92–100, 2014.

[26] J. N. BeMiller, "Monosaccharides," in *Carbohydrate Chemistry for Food Scientists*, 3rd ed., J. N. BeMiller, Ed. Elsevier Inc., 2019.

[27] R. E. Masithoh, H. Z. Amanah, W. S. Yoon, R. Joshi, and B. K. Cho, "Determination of protein and glucose of tuber and root flours using NIR and MIR spectroscopy," 2020.

[28] W. H. Su and D. W. Sun, "Potential of hyperspectral imaging for visual authentication of sliced organic potatoes from potato and sweet potato tubers and rapid grading of the tubers according to moisture proportion," *Comput. Electron. Agric.*, vol. 125, pp. 113–124, 2016.